Influence of the inhomogeneous troposphere on GNSS positioning and integer ambiguity resolution

Ma, Hongyang; Psychas, Dimitrios; Xing, Xuhuang; Zhao, Qile; Verhagen, Sandra; Liu, Xianglin

DOI
10.1016/j.asr.2020.12.043

Publication date
2021

Document Version
Final published version

Published in
Advances in Space Research

Citation (APA)
Ma, H., Psychas, D., Xing, X., Zhao, Q., Verhagen, S., & Liu, X. (2021). Influence of the inhomogeneous troposphere on GNSS positioning and integer ambiguity resolution. *Advances in Space Research*, *67*(6), 1914-1928. https://doi.org/10.1016/j.asr.2020.12.043

Available online at www.sciencedirect.com

ScienceDirect

Advances in Space Research 67 (2021) 1914–1928

ADVANCES IN SPACE RESEARCH (a COSPAR publication)

www.elsevier.com/locate/asr

Influence of the inhomogeneous troposphere on GNSS positioning and integer ambiguity resolution

Hongyang Ma [a,b,*], Dimitrios Psychas [b,c], Xuhuang Xing [d], Qile Zhao [a,*], Sandra Verhagen [b], Xianglin Liu [c]

[a] GNSS Research Center, Wuhan University, Wuhan 430079, China
[b] Department of Geoscience and Remote Sensing, Delft University of Technology, Delft 2600 AA, the Netherlands
[c] Fugro Innovation & Technology B.V., Leidschendam 2631 RT, the Netherlands
[d] Hainan Meteorological Service Center, Haikou 570203, China

Received 11 September 2020; received in revised form 27 December 2020; accepted 31 December 2020
Available online 9 January 2021

Abstract

The tropospheric delay is one of many error sources that affect the Global Navigation Satellite System (GNSS) positioning solutions. The widely used troposphere models assume a homogeneous atmosphere so that only the zenith delay needs to be determined and is mapped through an elevation-dependent mapping function. This procedure is to reduce the computational burden and keep the positioning model full-rank. However, this assumption fails for a realistic description of the troposphere, which is always asymmetrical at a certain elevation angle, especially during a weather event when the weather conditions are very complex. These imperfectly modelled tropospheric delays may influence the positioning accuracy and integer ambiguity resolution performance. In this case, this contribution aims to investigate the effects of the model errors due to the asymmetrical troposphere on GNSS estimations. The Numerical Weather Prediction (NWP) model is applied to generate the actual ray-tracing tropospheric delay in Western Europe, and the tropospheric model errors are calculated in a normal weather condition and a weather event condition by comparing the slant delay calculated from the NWP model and the mapping function. Case studies on the same GNSS station are conducted in two weather conditions: a normal troposphere condition and a weather event with heavy rainfall. The results based on the case studies show that the troposphere in the normal weather condition is nearly homogeneous that the azimuthal-dependent discrepancies of the tropospheric delay are less than 1cm at a very low elevation angle; meanwhile, the discrepancies between different azimuthal angles can reach to more than 25cm in the weather event. A single-frequency Single Point Positioning (SPP) model and a Precise Point Positioning (PPP) model that preserves the integer property of ambiguity are chosen for studying the estimation biases caused by the troposphere model errors. It turns out that almost all horizontal positioning biases of SPP and PPP are less than 1cm in the normal weather condition; however, the scales of the horizontal and 3D biases are concentrated in 1 to 10cm in the weather event for these two models. This contribution also contains the study of the actual integer ambiguity resolution success rate in the presence of the tropospheric model errors by applying the Monte Carlo simulation, and the success rates of PPP in the normal weather condition are consistent with the theoretical values calculated with the ideal troposphere which is totally symmetrical. However, the actual success rates in the weather event are extremely low at some epochs due to the tropospheric model errors, which means that wrong fixing may occur since the theoretical values cannot take into account these model errors. Note that the horizontal tropospheric gradients are not involved in the processing, which means that an optimistic performance might be expected if the gradients are considered.

Keywords: GNSS; Tropospheric delay; PPP; PPP-AR; Integer ambiguity resolution; Monte Carlo simulation; Model errors

* Corresponding authors.
E-mail addresses: h.ma-3@tudelft.nl (H. Ma), d.psychas@fugro.com (D. Psychas), zhaoql@whu.edu.cn (Q. Zhao), Sandra.Verhagen@tudelft.nl (S. Verhagen), xianglin.liu@fugro.com (X. Liu).

https://doi.org/10.1016/j.asr.2020.12.043
0273-1177/

1. Introduction

Global Navigation Satellite System (GNSS) has the advantages of all-weather-capability, high accuracy and low-cost realization and thereby is an ideal tool for positioning. Single Point Positioning (SPP) and Precise Point Positioning (PPP) utilizing undifferenced observations to perform positioning at worldwide scales are two important applications of GNSS (Zumberge et al. 1997). SPP and PPP have the advantage of being able to deploy by using a single receiver and therefore been widely used in geodetic positioning applications because its operating scope is not restricted by simultaneous observations from any other stations.

Model errors are crucial for GNSS data processing. On the one hand, the positioning solutions might be biased by the existence of such errors. For instance, due to the high correlation between the vertical direction and the tropospheric delay, the accuracy of the up component would be affected if the tropospheric delay is not well modelled. On the other hand, the float ambiguities may not be successfully fixed to integer values in the presence of the model errors for the integer ambiguity resolution enabled PPP, leading to wrongly resolved ambiguities and causing large positioning errors. In such a case, the fixed solutions with wrong integer ambiguities are even worse than the float solutions (Verhagen et al., 2013). This integer ambiguity resolution enabled PPP is referred to as the PPP-AR in the following discussions, and it can improve the positioning accuracy as well as reduce the convergence as compared to the standard PPP. Plenty of methods and strategies aiming to make use of the integerness of the ambiguity in a single receiver have been proposed by taking the corrections of the hardware delays into account during the last decades (Wübbena et al., 2005; Ge et al., 2008; Bertiger et al., 2010; Teunissen et al., 2010; Geng et al., 2011; Odijk et al., 2016; Psychas et al., 2018; Zhang et al., 2019).

Among others, the tropospheric delay is one of the major error sources in GNSS positioning, and it can cause an offset about 2.3m in the zenith direction at sea level and reach up to several tens of meters at a low elevation angle. Although 90% of the total tropospheric delay, i.e., the hydrostatic delay can be well modelled and compensated with empirical tropospheric models (Saastamoinen, 1972; Leandro et al., 2006; Boehm et al., 2007; Yao et al., 2015), the wet part of troposphere is less accurately predictable due to the high spatial and temporal variability of water vapor. Therefore, the wet delay corrections from an empirical model would not be accurate enough for practical use. Thus, the tropospheric wet delay is usually estimated at zenith direction and then mapped to slant directions using an elevation-dependent mapping function (Ifadis, 1992; Niell, 1996; Boehm et al., 2006; Landskron and Boehm, 2018).

However, the zenith-delay-plus-mapping-function procedure only works well under the assumption of an azimuthal symmetric atmosphere around the receiver. Due to local and regional climatic and weather conditions, the tropospheric delay at a constant elevation angle would slightly vary with the different azimuth directions. This asymmetrical troposphere would become more evident in a weather event due to the complex climatological conditions, e.g., heavy rainfall, storms and typhoons (Ma and Verhagen, 2020). Li et al., (2014) investigated the impacts of the troposphere model errors on the integer ambiguity resolution; however, only the model errors at the zenith direction are considered and simulated.

To analyse the impact of the asymmetrical atmosphere, the so-called horizontal tropospheric gradients were proposed to be estimated together with the zenith delay for utmost precise positioning applications (Bar-Sever et al., 1998; Boehm and Schuh, 2007; Steigenberger et al., 2007). However, the mapping function is still needed when implementing the horizontal tropospheric gradients, and in this case, a tilted direction instead of the zenith is introduced for mapping slant tropospheric delays (Meindl et al., 2004). In such a case, the practical performance of the gradients would be limited in weather events since the horizontal tropospheric gradients only consider the first order asymmetry of the troposphere in north–south and east–west direction (Chen and Herring, 1997). Dousa et al. (2016) proved that the GNSS-derived gradients could only demonstrate the asymmetrical troposphere during a homogeneous gradient field. Masoumi et al. (2017) also illustrated that the traditional horizontal tropospheric gradients performed well in a normal tropospheric situation but failed to accurately model asymmetrical troposphere in abnormal weather conditions with existing the isolated gradients in some directions. Therefore, the asymmetrical troposphere may still be a threat to precise positioning solutions in weather events. As this study does not implement the gradients, an optimistic performance in a normal weather condition would be expected if these parameters are considered. However, the positioning solutions and integer ambiguity resolution during a weather event may still suffer from the asymmetrical troposphere.

The NWP model is a useful tool to analyse the influence of the troposphere because it contains all meteorological information necessary for computing the ray-traced hydrostatic and wet delay, e.g., temperature, pressure, water vapor content and liquid. Many of the well-known troposphere models or mapping functions are based more or less on the data from NWP models. The HARMONIE (Hirlam Aladin Regional on Meso-scale Operational NWP In Europe) is a non-hydrostatic spectral high-resolution limited area model with a model grid up to 1km resolution in the horizontal plane and 65 vertical levels and has been implemented and utilized in some European countries (de Haan et al., 2013). It uses initial state obtained through multi-sensors as input to predict the weather conditions and can provide the complete description of the neutral atmosphere. Therefore, it is ideally suited to determine the ray-traced tropospheric delays in a regional area.

This contribution aims to investigate the influence of the asymmetrical troposphere on GNSS positioning and integer ambiguity resolution. The tropospheric model errors caused by the inhomogeneous atmosphere are obtained by comparing the slant delays from the NWP model and the mapping function. This article is organized as follows. Section 2 presents the theory of retrieving slant tropospheric delays from the NWP model, which are referred to as the true tropospheric delay values. Then the tropospheric model errors in two weather conditions, a normal weather and a weather event, are obtained by comparing the slant delays from the NWP model and the mapping function. Section 3 illustrates the influence of the asymmetrical troposphere errors on the single-frequency SPP positioning solutions, i.e., the least-squares estimator is applied at each epoch without any dynamic information. Section 4 reviews the integer ambiguity resolution enabled PPP positioning concept along with the method of fixing integer ambiguity; a PPP-AR model is introduced for which ambiguities can preserve the integer nature and thus can be fixed to integer values. The influence of the inhomogeneous troposphere on the positioning solutions is investigated in this section, as well as its impacts on integer ambiguity resolution. Section 5 contains the conclusions and discussions.

2. Retrieving tropospheric delays from NWP model

NWP models apply the atmospheric parameters obtained from multiple sensors in a regional area to describe a realistic tropospheric delay in slant directions. The HARMONIE model has been developed and optimized for European weather conditions and thereby running at Royal Netherlands Meteorological Office (KNMI). The slant tropospheric delay (STD) in this NWP model is calculated by

$$\mathrm{STD} = 10^{-6}\int_{\mathrm{R}}^{\mathrm{S}} \mathrm{N(x)dx} \tag{1}$$

where N is the so-called refractivity of the atmosphere; dx is an infinitesimal distance along the true ray path. The geometry distance which connects S the transmitter and R the receiver is the ray-path. Note that this ray-path may not be a straight line due to the tropospheric bending effects. The real part of the refractivity N is calculated using the empirical Smith and Weintraub model (Smith and Weintraub, 1953)

$$\mathrm{N} = \mathrm{k}_1 \cdot \frac{\mathrm{p_d}}{\mathrm{T}} + \mathrm{k}_2 \cdot \frac{\mathrm{p_w}}{\mathrm{T}} + \mathrm{k}_3 \cdot \frac{\mathrm{p_w}}{\mathrm{T}^2} \tag{2}$$

where T is temperature given in Kelvin; p_d and p_w are the partial pressure of dry air and water vapor in hPa, respectively; k1, k2 and k3 are of constant values which can be found in Bevis et al. (1994). The term with p_d and p_w is relating to hydrostatic refractivity and wet refractivity, respectively. The parameters T, p_d and p_w are part of the HARMONIE analyses and thus can be used to compute the refractivity N. In addition, the climatological information can be obtained through a global pressure and temperature model in case the GNSS receiver is not equipped with any meteorological sensors or NWP models are not available (Boehm et al., 2007; Lagler et al., 2013).

The date of 31-May-2018 is selected with the weather events of heavy rainfall and thunderstorm, which is referred to as the weather event day; meanwhile, a normal weather day of 08-April-2019 is selected as the comparison, which is referred to as the normal weather day. The zenith hydrostatic and wet delay of the normal weather day and the weather event day can be seen in Fig. 1 and Fig. 2, respectively.

The zenith hydrostatic delays in these two weather conditions are almost the same. This is because the hydrostatic delay is mainly caused by the refractivity of the dry gases and solely dependent on atmospheric pressure. As the atmospheric pressure remains nearly invariant above the sea level but varies in orography area, a fairly good agreement for the coastline and the zenith hydrostatic delay can be seen between the sea and inland areas. The wet delays, on the contrary, are large in the weather event day as compared to the normal weather because the water vapor is responsible for most of the wet delays. Therefore, the following discussions will focus on the tropospheric wet delay due to its sensitivity to water vapor content.

Another way to model the satellite-dependent tropospheric delay is using mapping function projecting tropospheric delay from zenith to any elevation angles. In this study, the Ifadis mapping function is applied for its relatively easy implementation and high precision (Ifadis, 1992).

$$m_u^s(e) = \frac{1}{\sin(e) + \frac{a}{\sin(e) + \frac{b}{\sin(e)+c}}} \tag{3}$$

where c is a constant value of 0.078 while a and b are temperature and water vapor content dependent parameters; e denotes the elevation angle of a certain satellite. As can be seen in elevation-dependent Eq. (3) that this function assumes a homogeneous and spherically stratified atmosphere for computational convenience.

The GNSS station ADR2 is chosen to investigate the discrepancies of the slant wet delays calculated with NWP model of Eq. (1) and the Ifadis mapping function of Eq. (3). The location of ADR2 is shown in the weather event of Fig. 2 that the station is on a precipitating line. Therefore, the GNSS data of this station must suffer from the weather event and thus become an ideal dataset for investigating the tropospheric influence. The slant wet delays of the normal weather day and weather event day obtained from the NWP model and the zenith wet delay with the mapping function and are shown in Fig. 3. The red dash represents the tropospheric delay calculated by the elevation-dependent mapping function, and the solid lines represent the elevation-and-azimuth-dependent tropospheric delay obtained from the NWP model. Note that

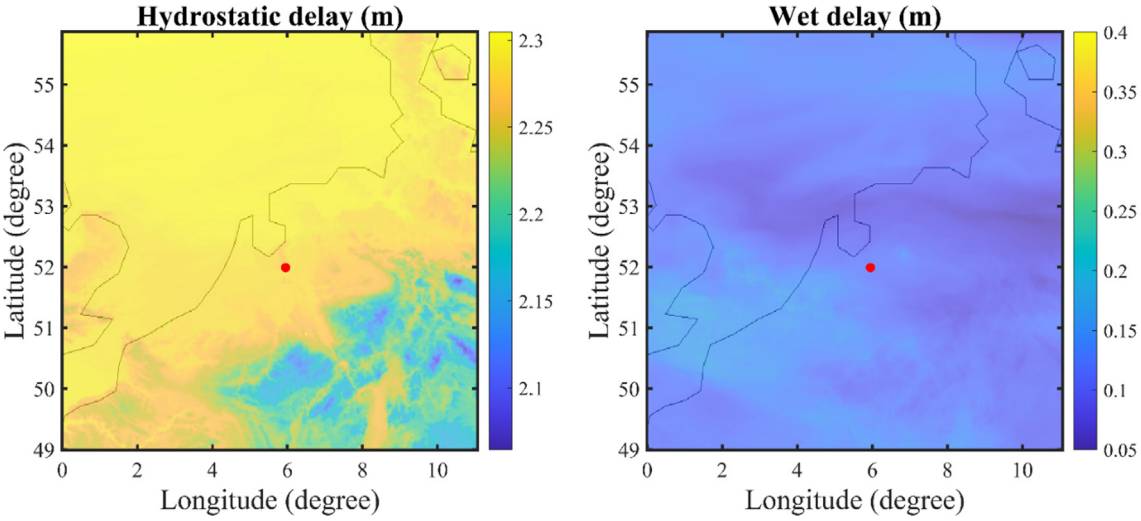

Fig. 1. Zenith hydrostatic and wet delay in normal weather day. The red dot is the GNSS station ADR2. (For interpretation of the references to color in this figure legend, the reader is referred to the web version of this article.)

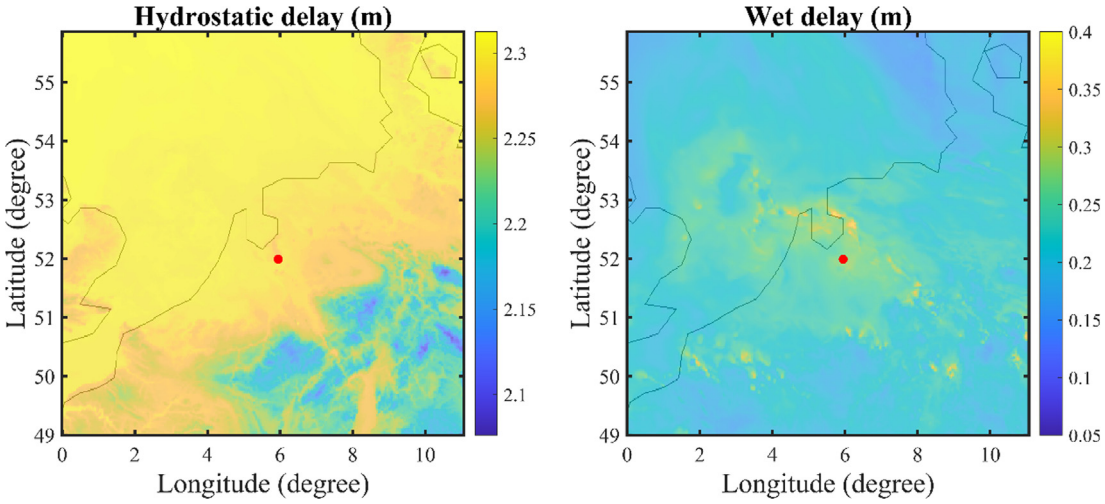

Fig. 2. Zenith hydrostatic and wet delay in weather event day. The red dot is the GNSS station ADR2. (For interpretation of the references to color in this figure legend, the reader is referred to the web version of this article.)

each solid line indicates one azimuth angle from 0 to 360° in an interval of 10°.

It can be seen in Fig. 3 that the pattern of the mapped tropospheric delay is in accordance with the NWP retrieved delay because the coefficients of the Ifadis mapping function are also based on the data of NWP models. The tropospheric delay is increasing with the decreasing elevation angles since the signal path in the troposphere is longer when the satellite is at low elevation angles. As for the normal weather day, the tropospheric delays at different azimuth angles are distinguishable only when the elevation angles are very low, e.g., below 15°, which means that the assumption of symmetrical troposphere is realistic for normal weather, and thus the zenith-delay-plus-mapping-function procedure can work well.

As for the weather event day, on the contrary, the distinguishable NWP tropospheric delays in different azimuthal angles can be seen at relatively high elevation angles, e.g., 40–50°. This is because the weather front passing through may cause dramatic variations of the water vapor contents, and thereby signals coming from different directions may suffer from different tropospheric wet delays. Besides, the large scales of the tropospheric delay values in the weather event day are due to the presence of the large amounts of water vapor, therefore, the discrepancies of the tropospheric delays between the mapping function and NWP model would be more significant than those of in the normal weather day, as can be seen in Fig. 4.

Fig. 4 presents that the asymmetrical tropospheric delay varies in azimuth and is less than 1cm for most of the cases in the normal weather day. However, the discrepancies can even exceed 25cm during the weather event, and these unmodelled tropospheric delays should have substantial influences on data processing. In this case, we will investi-

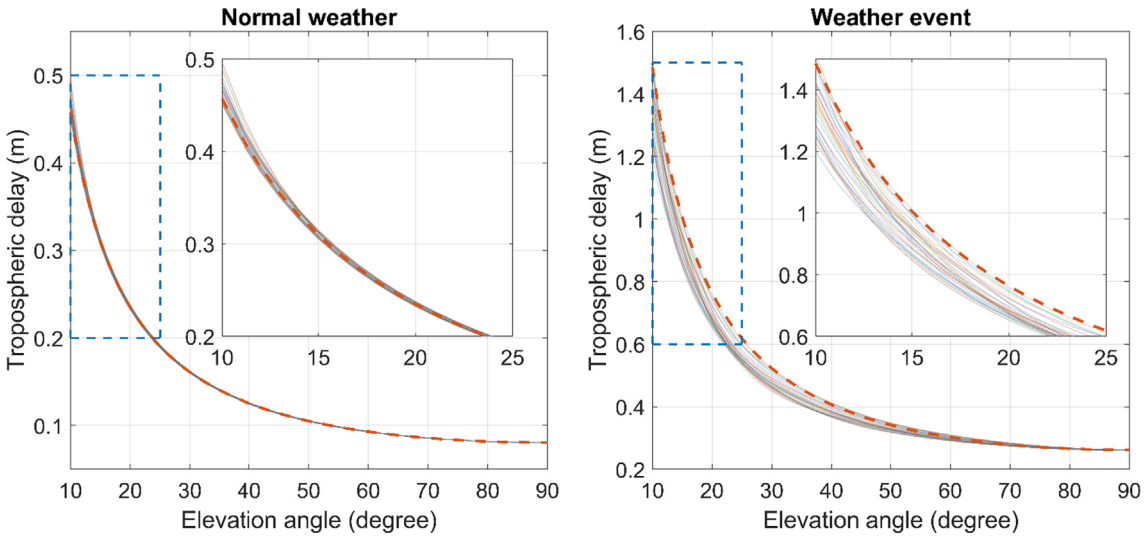

Fig. 3. Slant wet delays obtained from the mapping function (red dash) and the NWP model (solid lines). Each solid line represents an azimuth angle from 0 to 360° in an interval of 10°. (For interpretation of the references to color in this figure legend, the reader is referred to the web version of this article.)

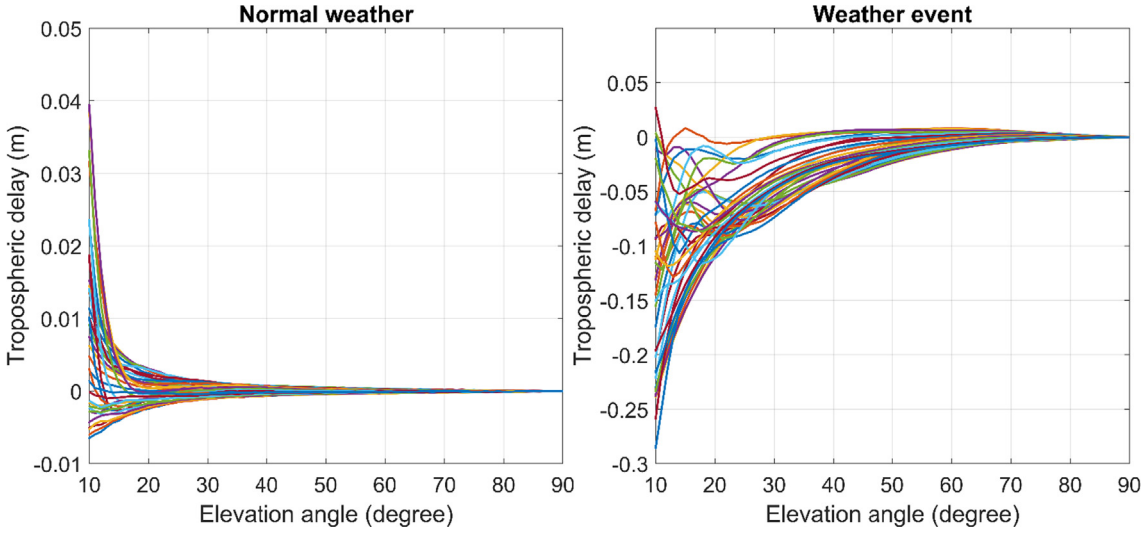

Fig. 4. Discrepancies of the tropospheric delay between mapping function and NWP model. Each solid line represents an azimuth angle from 0 to 360° in an interval of 10°.

gate the impacts of the inhomogeneous troposphere on GNSS estimations in the following two sections.

3. Influences of the asymmetrical troposphere on SPP

One of the simplest positioning strategies is the Single Point Positioning in which single-frequency pseudo-range observations measured by one receiver are processed to solve for its position. This technique is widely used in some scenarios that are insensitive to precision, e.g., pedestrian navigation (Knoop et al., 2017; Psychas et al., 2019) and mountainous area where the precise satellite orbit and clock corrections are not available (Angrisano et al., 2013). The single-frequency code-based SPP model reads

$$\mathrm{E}\{\Delta p_u^s\} = {g_u^s}^{\mathrm{T}} \Delta x_u + dt_u \quad (4)$$

where $\mathrm{E}\{\cdot\}$ is the expectation operator; Δp_u^s is the so-called observed-minus-computed from satellite s to user receiver u; the satellite clock offset has been compensated by the a priori corrections; g_u^s denotes the line-of-sight unit vector from the satellite to the receiver; Δx the increment of the receiver position; dt_u is the receiver clock offset. The ionospheric delay is assumed to be corrected by the empirical models, e.g., Klobuchar (Klobuchar, 1987) or Global Ionosphere Maps (Schaer et al., 1998). In this case, only four unknowns are involved in the observation equation and at least 4 satellites need to be tracked at each epoch to solve Eq. (4).

To facilitate the interpretation, the linearized user model of Eq. (4) can be compactly presented as

$$\mathrm{E}(y) = Ax, \mathrm{D}(y) = Q_{yy} \quad (5)$$

where y represents the vector of code measurements corrected for the satellite clock offsets; x and A are the estimable parameters and the corresponding design matrix, respectively. D{·} denotes the mathematical dispersion operation, and Q_{yy} denotes the variance matrix of the observations. We assume that the imperfectly modelled tropospheric delay due to the inhomogeneous atmosphere will cause an error vector Δy, and the estimates will be biased after applying the best linear unbiased estimator

$$\Delta\hat{x} = \left(A^T Q_{yy}^{-1} A\right)^{-1} A^T Q_{yy}^{-1} \Delta y \quad (6)$$

where $\Delta\hat{x}$ is the biased estimates due to the imperfectly modelled tropospheric delay. Therefore, the positioning errors due to the unmodelled tropospheric delay can be obtained directly.

We first investigate the influence of the troposphere model errors caused by the asymmetrical atmosphere on the single point positioning, which means that, as can be seen in Table 1 the strategy of data processing, the unknown parameters are estimated on an epoch-by-epoch basis. The GNSS station ADR2 is used to provide the receiver-satellite geometry.

Since we have known the discrepancies between mapping function based tropospheric delays and NWP model based tropospheric delays, the tropospheric model error for each satellite can be obtained from Fig. 4 with the information of elevation and azimuth angle, which formulate the error vector Δ*y*. The left panel of Fig. 4 represents the magnitude of the model errors in normal weather day, and the right panel of Fig. 4 represents the weather event day. All these tropospheric model errors are assumed exist in the whole day for simple implementation. With the model error vector Δ*y*, the biased least-squares estimates are calculated by Eq. (6); therefore, the positioning errors can be analyzed.

Fig. 5 presents the horizontal and absolute vertical positioning biases due to the asymmetrical troposphere in normal weather day and weather event day along with the Horizontal Dilution of Precision (HDOP) and Vertical Dilution of Precision (VDOP), which are calculated by Eq. (7).

$$HDOP = \sqrt{\sigma_E^2 + \sigma_N^2} \quad (7)$$

$$VDOP = \sqrt{\sigma_U^2}$$

where σ_E^2, σ_N^2 and σ_U^2 are the covariances of east, north and up component, respectively.

Note that since this study does not use real data, the normal weather case and weather event case apply the same receiver-satellite geometry from the GNSS station ADR2 on 8th April 2019. Therefore, the DOPs are identical for both the normal weather and weather event cases in Fig. 5 and following corresponding figures. With the identical DOPs, it would be straightforward to compare the differences under the normal weather and the weather event.

The scales of the positioning biases on both horizontal and vertical component exhibit good correspondence with the DOP values because the model errors would have a large impact on estimations when the receiver-satellite geometry is not strong. The influence of the asymmetrical troposphere in the normal weather condition can nearly be neglected due to the very small biases that the 3D positioning biases, as shown in Fig. 6, are less than 0.5 cm and 1 cm with 92.95% and 97.81% probability, respectively. Besides, it is reasonable to see significant biases caused by the weather event which are larger than 5 cm and 10 cm with 55.35% and 8.72% probability, respectively. However, these biases may still be accepted if the SPP users pursue meter-level positioning accuracy. As for the decimeter-level accuracy SPP (Pelc-Mieczkowska and Tomaszewski, 2020), users should be aware of the SPP performances during weather events.

4. Influences of the asymmetrical troposphere on PPP and integer ambiguity resolution

One drawback of PPP is that the ambiguities cannot be fixed into integer values due to the existing satellite and receiver hardware delays, and a fairly long solution convergence is needed. Consequently, successful integer ambiguity resolution becomes one of the key factors contributing to GNSS high precision positioning.

An undifferenced and uncombined PPP-AR model is used in this study because it takes advantage of the straightforward observation variance–covariance matrix and remains all estimable parameters for a possible further model strengthening as, for instance, by providing external ionospheric corrections to achieve near-instantaneous

Table 1
Summary of the strategy of single point positioning.

Parameter	Strategy and value
Positioning mode	Epoch by epoch
Constellation	GPS
Data	L1 and L2 code-only
Interval	30 s
Elevation cutoff angle	10°
Weighting strategy	Elevation dependent
Standard deviation of code observable	0.5 m
Study cases	Normal weather day and weather event day

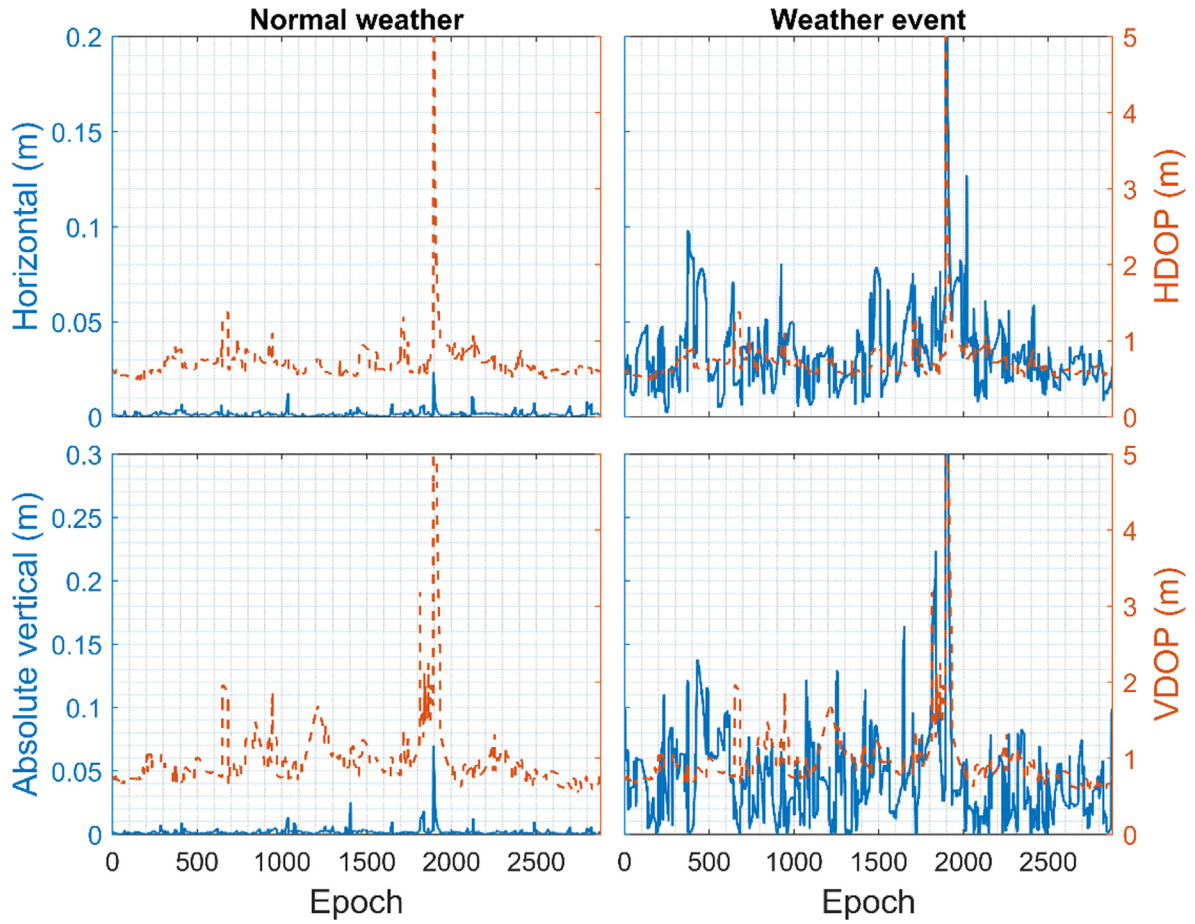

Fig. 5. Horizontal and vertical positioning biases due to the asymmetrical troposphere in normal weather day and weather event day in SPP mode.

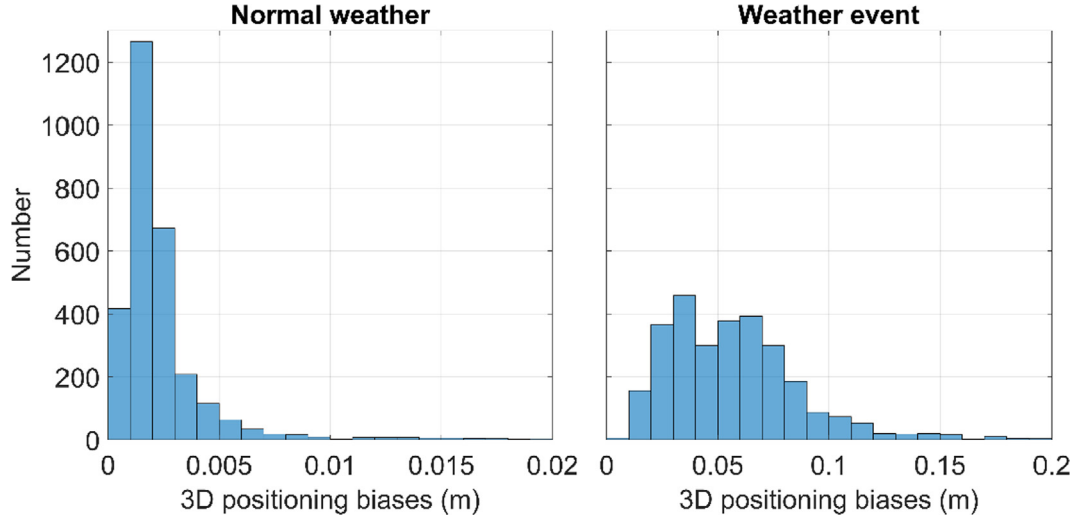

Fig. 6. Histogram of 3D positioning biases caused by the asymmetrical troposphere in normal weather and weather event condition in SPP mode.

high-precision positioning (Psychas and Verhagen, 2020). We simply provide the reader with the positioning equations at the user side, and a detailed review and extension of this model can be found in (Teunissen et al., 2010; Odijk et al., 2016; Ma et al., 2020).

$$\mathrm{E}\left\{\Delta\phi^{s}_{u,j}\right\} = g^{s\,T}_{u}\Delta x_{u} + m^{s}_{u}\tau_{u} - \mu_{j}\imath^{s}_{u} + dt_{u} + \delta_{u,j} + \lambda_{j}z^{s}_{u,j} \quad (8)$$

$$\mathrm{E}\left\{\Delta p^{s}_{u,j}\right\} = g^{s\,T}_{u}\Delta x_{u} + m^{s}_{u}\tau_{u} + \mu_{j}\imath^{s}_{u} + dt_{u}$$

where τ_u denotes the zenith tropospheric delay and m_u^s its corresponding mapping function which introduces an elevation-dependent scaling factor for each satellite; I_u^s is the slant ionospheric delay on the first frequency and having μ_j as the coefficient; $\Delta\phi_{u,j}^s$ is the so-called observed-minus-computed phase observation, in meters; $\delta_{u,j}$ is the receiver phase bias, in meters; λ_j denotes the wavelength and $z_{u,j}^s$ the integer ambiguity, in cycles; the rest of the notations $\Delta p_{u,j}^s$, $g_u^{s\,T}$, Δx_u, and dt_u have the same interpretations as in Eq. (4). Note that the satellite clock offsets as well as the satellite phase biases have been compensated through the a priori corrections, and the receiver phase biases separated from the ambiguities, which ensures the integerness of the ambiguities.

The model strength and the applied integer estimator are two crucial factors for successful and reliable ambiguity fixing, and the integer ambiguity resolution success rate plays an important role in measuring the model strength. After attaining the estimates and the corresponding variance–covariance (VC) matrix from Eq. (8), we further assume the float ambiguity resolution is $\hat{z}$ and its VC matrix $Q_{\hat{z}\hat{z}}$, and the float ambiguity vector is normally distributed as $\hat{z}\ N\left(z, Q_{\hat{z}\hat{z}}\right)$ for which z is the unbiased integer ambiguity resolution. However, the float ambiguity estimations are affected by the unmodelled tropospheric delay with the bias Δz, which leads to

$$\hat{z}\ N\left(z + \Delta z, Q_{\hat{z}\hat{z}}\right) \tag{9}$$

Since we have obtained the estimation and distribution of the float ambiguity resolution, the integer ambiguity success rate can be modelled by Monte Carlo simulation. Verhagen et al. (2013) confirmed that if the number of samples is sufficiently large, e.g., more than 10^5, the Monte Carlo based success rate can give a very good approximation to the lower bound of the integer least-squares estimator. In this study, the true ambiguity vector z is assumed to be 0, and then 10^5 samples are simulated with the distribution $N\left(0, Q_{\hat{z}\hat{z}}\right)$ with the ideal troposphere for which no model errors are appeared and $N\left(\Delta z, Q_{\hat{z}\hat{z}}\right)$ with the realistic troposphere condition in normal weather and weather event. The simulated success rate is the ratio between the number of correctly simulated ambiguity vector (0 vector) and the number of samples (10^5).

By considering the dynamic behaviour of the unknown parameters, PPP can reach centimetre level positioning accuracy after accumulating a certain number of observations. While at the same time, the integer ambiguity resolution success rate would be increasing with the strengthening model. The configuration of the dynamic parameters can be seen in Table 2. The coordinates will be estimated in kinematic and static mode, respectively. The receiver clock offset, as well as the ionospheric delay are considered as epoch-wise estimation due to their high variabilities. The tropospheric delay is highly constrained because the troposphere is stable in time during a normal weather condition. The receiver phase delay and the ambiguity are considered as constant values over time.

In general, most of the PPP data processing implements the Kalman filter, which is a recursive method to estimate the random states of a dynamic system in a way that minimizes the mean squared prediction error (Verhagen and Teunissen, 2017). However, the estimation biases of the parameter with a dynamic model at the current epoch may be accumulated to the next epoch. In other words, by using Eq. (6), we can obtain the estimation biases at the first epoch

$$\Delta\hat{x}_{0|0} = \left(A^T Q_{yy}^{-1} A\right)^{-1} A^T Q_{yy}^{-1} \Delta y_0 \tag{10}$$

where $\Delta\hat{x}_{0|0}$ indicates the estimation biases at the initial epoch caused by the troposphere model error Δy_0. Then these biases will be accumulated to the next epoch through the time update

$$\Delta\hat{x}_{k|k-1} = \Delta\hat{x}_{k-1|k-1} \tag{11}$$

where $\Delta\hat{x}_{k-1|k-1}$ is the estimation biases at $k-1$ epoch, and $\Delta\hat{x}_{k|k-1}$ is the predicted biases at epoch k, which is involved in the predicted state $\hat{x}_{k|k-1}$. Here we assume the transition matrix is the identity matrix because the dynamic system is described by the differential equations of the first-order linearized positioning model. In this case, the prediction residual Δv_k is biased by

$$\Delta v_k = \Delta y_k - A_k \Delta\hat{x}_{k|k-1} \tag{12}$$

Finally, the estimation biases at epoch k is given as

$$\Delta\hat{x}_{k|k} = \Delta\hat{x}_{k|k-1} + K_k \Delta v_k \tag{13}$$

where K_k is the so called Kalman gain which can be calculated in the Kalman filter process. Similar to the SPP experiment, the influence of the asymmetrical troposphere on the positioning results and integer ambiguity resolution are analyzed once the estimation biases are obtained.

Fig. 7 presents the horizontal and vertical positioning biases due to the asymmetrical troposphere in the normal weather and weather event condition in kinematic PPP, which means that the receiver positions between the neighboring epochs are independent. The DOP values are small compared to those of SPP because the model strength is being improved with the increasing observations. However, the magnitude of the positioning biases of the kinematic PPP is not better than that of SPP because the DOP only represents the model strength but is not able to deal with potential model errors.

In general, the positioning biases caused by the asymmetrical troposphere in normal weather condition remain small. As shown in Fig. 8 the histogram of the 3D positioning errors in normal weather condition, 89.03% of which are less than 0.5 cm and 97.92% are less than 1 cm, which are acceptable if one requires a centimeter level accuracy. However, The influences of the troposphere model errors

Table 2
Configuration of the dynamic parameters.

Parameter	Strategy and value
Positioning mode	Kinematic/Static
Receiver clock	Epoch-wise
Tropospheric delay	Spectral density 0.0001 m^2/s
Ionospheric delay	Epoch-wise
Receiver phase delay	Constant
Ambiguity	Constant
Data	L1 and L2 phase and code
Standard deviation of phase/code observable	0.005 m/0.5 m
Integer ambiguity success rate	Monte Carlo simulation with the number of samples 10^5

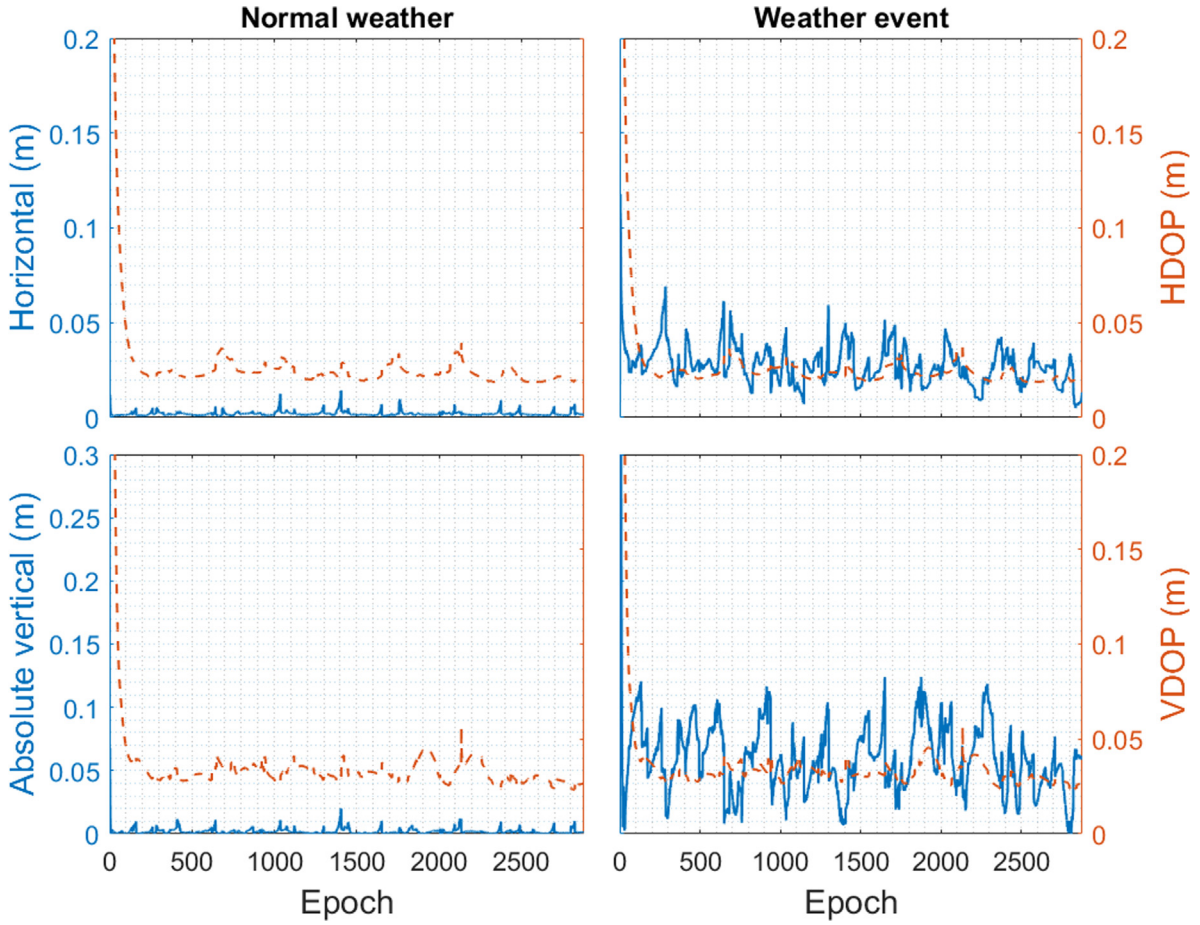

Fig. 7. Horizontal and vertical positioning biases due to the asymmetrical troposphere in normal weather day and weather event day in kinematic PPP mode.

in the weather event are much larger, as shown in Fig. 7 and Fig. 8. The 3D positioning biases are larger than 10 cm with 5.07% probability. It indicates that the solutions of kinematic PPP may not be reliable during weather events.

It is worth noting that the magnitude of the positioning biases of the kinematic mode is similar to the SPP results. This is because the estimates of position components are only dependent on the measurements of the current epoch as there are no dynamic models for the position parameters in kinematic mode. Although the number of observables of the kinematic mode is larger than that of the SPP model, the number of unknowns is also greater than the SPP, e.g., the additional tropospheric delays and ambiguities. Eventually, it turns out that the asymmetrical troposphere has almost the same influences on kinematic PPP and SPP.

With the strengthened model by accumulating observations, the ambiguities can be reliably fixed to integers once the success rate is sufficiently close to 1. Fig. 9 shows those success rates under the ideal troposphere without any asymmetrical influences and realistic troposphere in the normal weather and weather event conditions. The success

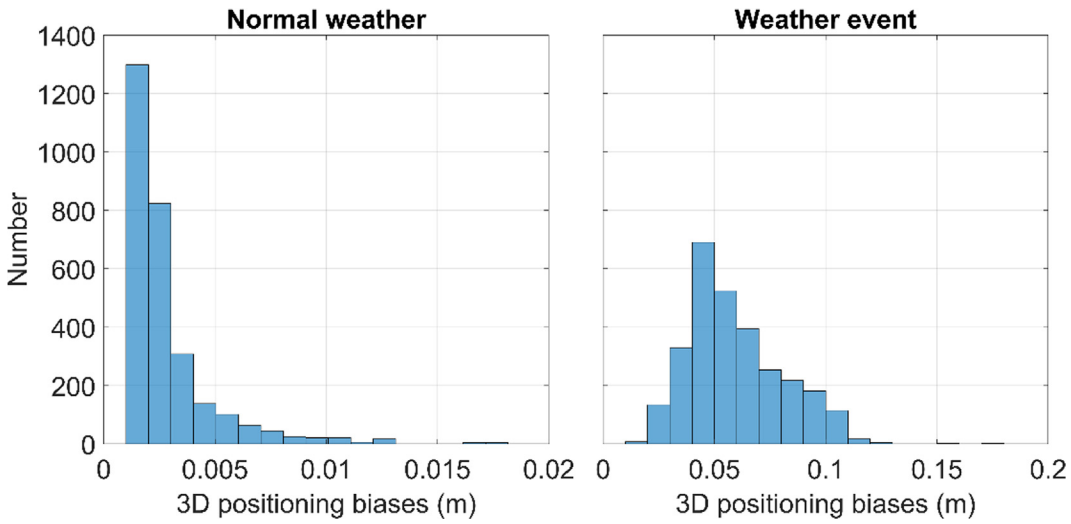

Fig. 8. Histogram of 3D positioning biases caused by the asymmetrical troposphere in normal weather and weather event condition in kinematic PPP mode.

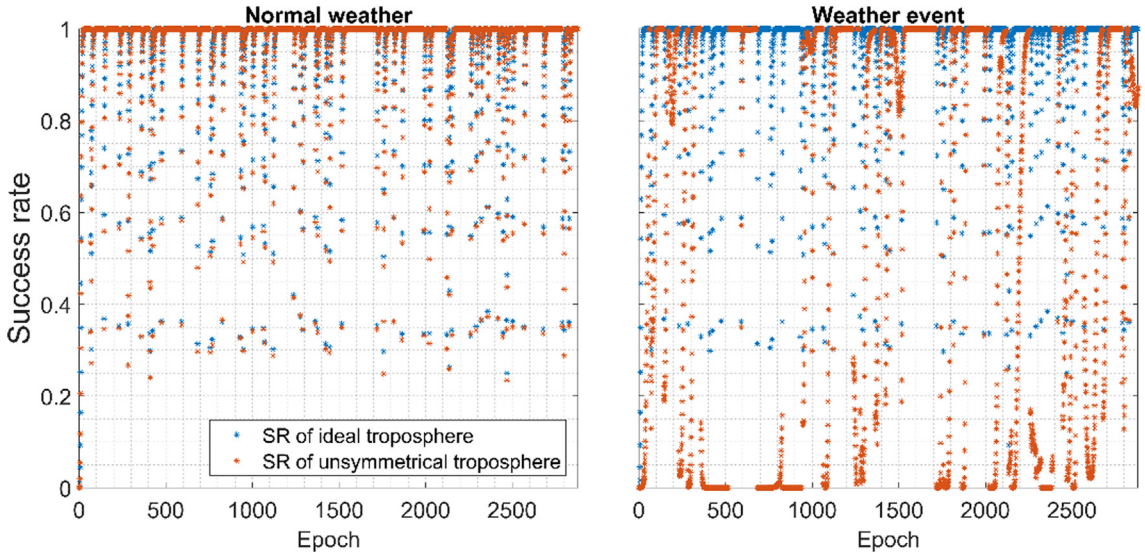

Fig. 9. Success rate (SR) of the full integer ambiguity resolution under ideal troposphere and realistic troposphere in kinematic PPP mode.

rates of the ideal troposphere represented by blue dots increases with the accumulation of epochs and approaches 1. Sometimes it drops down due to the new rising satellites since the full ambiguity resolution would be weakened by newly added ambiguities with fewer associated observations.

The success rates are not so much influenced by the inhomogeneous troposphere in the normal weather condition, which verifies a good assumption of simplifying atmosphere. However, the time series of the success rate during the weather event indicates that there is a large displacement compared with the ideal troposphere. In some periods, when the theoretical success rate under the ideal troposphere is close to 1, the success rate under the weather event, however, is very low or even at 0. This is because the influences of the model errors may be enlarged in the iteration of the Kalman filter process, as is shown in Eqs. (10)–(13). In other words, the advantage of the Kalman filter is considering the information of previous epoch at current epoch; however, at the same time, the estimations biases caused by model errors at the previous epoch would also involve in the current epoch along with the filter processing. Therefore, the accumulated ambiguity biases in kinematic data processing may influence the success rate simulated by Monte Carlo simulation. In this case, the ambiguities may not be correctly fixed, and thus the positioning solutions would consequently contain a large bias.

Note that the success rates can still reach high values even in the weather event. This usually occurs after a longer observation session compared to that of the ideal troposphere, and the success rate during the weather event drops dramatically when new satellites are considered in the posi-

tioning model, implying that the new ambiguities are easily affected due to the weak model strength.

As for the static PPP solutions for which the receiver is assumed to be stationary, the precision of the positioning results benefit from the strong model and thus the DOP values are extremely low, as shown in Fig. 10. The time series of the static positioning biases is stable as compared to those of the kinematic PPP or SPP. This is because the recursive positioning biases, along with the position parameters, are constrained by the dynamic model. The magnitudes of the positioning biases in the normal weather condition are around 0.5 cm with 3D and 0.1 cm with horizontal. However, one cannot ignore the positioning biases caused by the weather event since they are at the centimeter level, clearly an intolerable amount for the static PPP. For both normal weather and weather event case, the vertical biases are almost 5 times larger the horizontal biases because the tropospheric delay is highly correlated with the up component (see Fig. 11).

There is no doubt that the tropospheric model errors of normal weather condition have limited impacts on the success rate, as is shown in Fig. 12. The advantage of the stationary receiver does not improve the success rates in the weather event as the patterns of kinematic and static success rate in the realistic troposphere are nearly the same. The reason is that the dynamic model of estimating ambiguities is the same for the kinematic and static data processing, and the improvement of the model strength due to the static positions is insignificant for the ambiguities. This is also verified by Fig. 13, the ambiguity biases of the kinematic and static PPP caused by the asymmetrical troposphere in the weather event. One can see large biases on the newly added ambiguities due to the weak model strength, and the biases are reduced with the accumulation of observations. The simulated success rate is therefore continuously affected by these ambiguity biases.

5. Conclusions and discussions

The troposphere is one of the main error sources in GNSS positioning. The standard troposphere model assumes a homogeneous atmosphere for which only the zenith tropospheric delay needs to be estimated and then is mapped to ray-traced directions through an elevation-dependent mapping function. However, the assumption of the symmetrical troposphere is not realistic in GNSS applications, especially during weather events when the troposphere condition is complex.

The aim of this contribution is to investigate the influence of the model errors caused by the asymmetrical troposphere on positioning and integer ambiguity resolution. The NWP model is used to generate the slant tropospheric delays in the normal weather day and weather event day by integrating the refractivity at each signal arrival direction, then the tropospheric model errors are obtained by comparing the NWP ray-tracing delays and the mapped delays

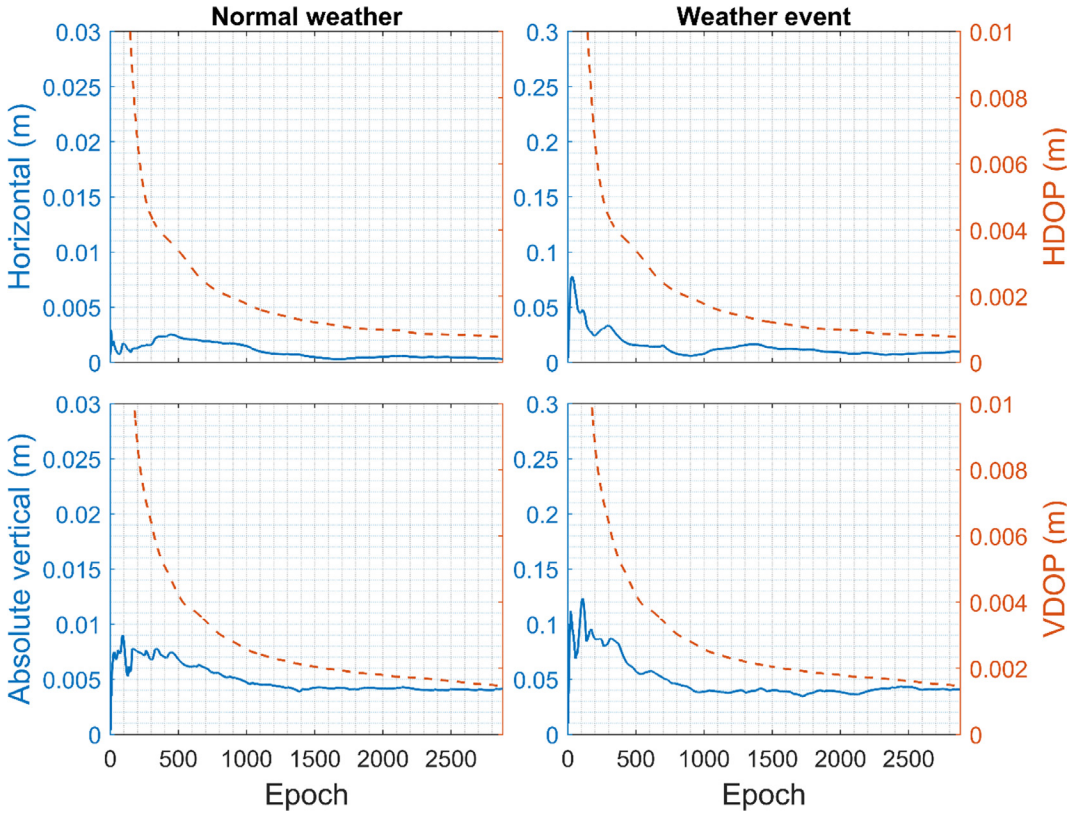

Fig. 10. Horizontal and vertical positioning biases due to the asymmetrical troposphere in normal weather day and weather event day in static PPP mode.

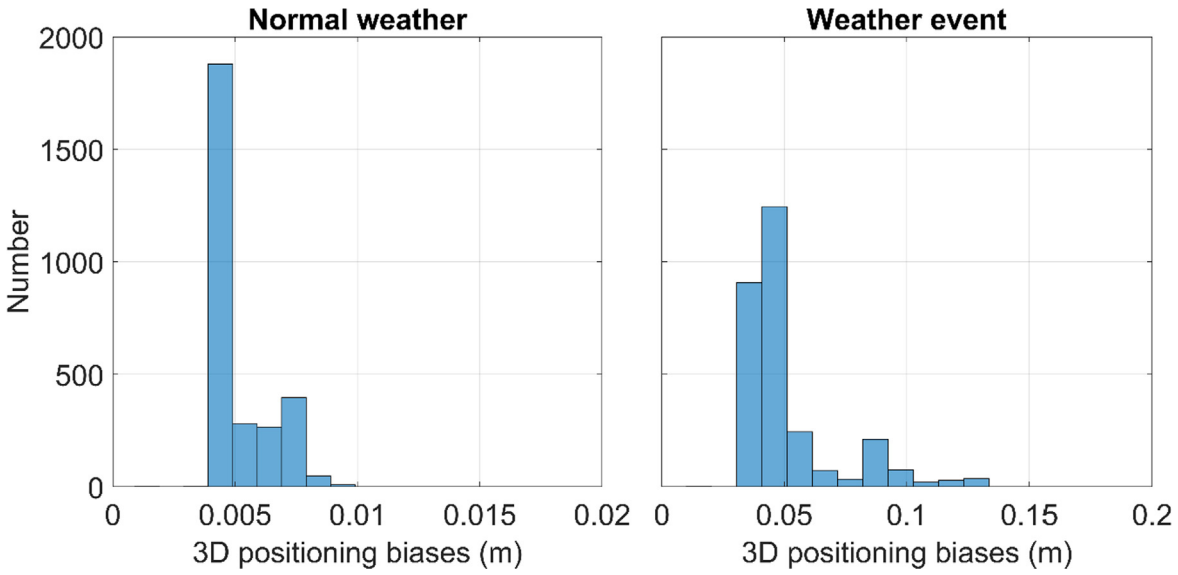

Fig. 11. Histogram of 3D positioning biases caused by the asymmetrical troposphere in normal weather and weather event condition in static PPP mode.

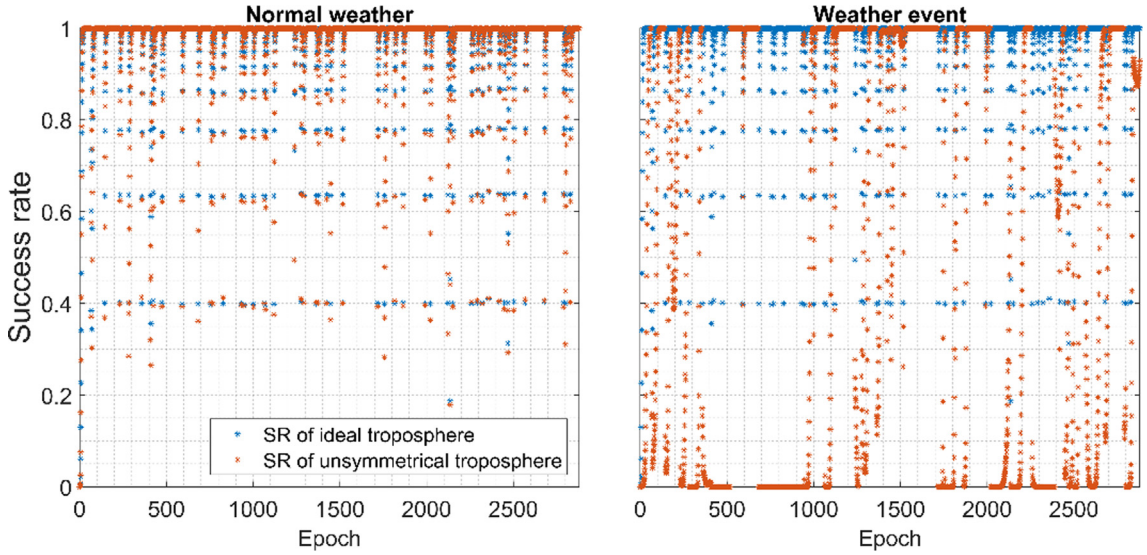

Fig. 12. Success rate (SR) of full integer ambiguity resolution under ideal troposphere and realistic troposphere in static PPP mode.

based on elevation angles only. The GNSS station at the centre of the experimental region is selected for providing the actual satellite-receiver geometry, and a single-frequency SPP model and an uncombined PPP-AR model is applied to evaluate the impacts of the tropospheric model errors on the selected station.

Both SPP based on epoch-by-epoch processing and PPP based on Kalman filter processing are applied in the experiments. The results, as presented in Table 3 the horizontal component, show that nearly all SPP and PPP positioning biases due to the inhomogeneous troposphere are less than 1cm in the normal weather condition. As for the weather event, however, the scale of the horizontal biases is at the centimeter level in one day's data processing. This is within an acceptable range for SPP which aims at meter-level positioning accuracy, but intolerant for PPP pursuing centimeter level accuracy or some decimeter-level accuracy SPP.

Table 4 presents the 3D ambiguity float positioning biases for which the up component has been taken into account. It is worth noting that the performance of the 3D positioning biases of PPP in the asymmetrical troposphere is not evidently better than that of the SPP because the biases will be accumulated to the next epoch in the recursive data processing. In other words, the estimations biases caused by model errors at the previous epoch would also involve in the current epoch along with the filter iteration.

Due to the presence of the biases in estimations, the integer ambiguity resolution success rate must be influenced, and the Monte Carlo simulation is applied to calculate

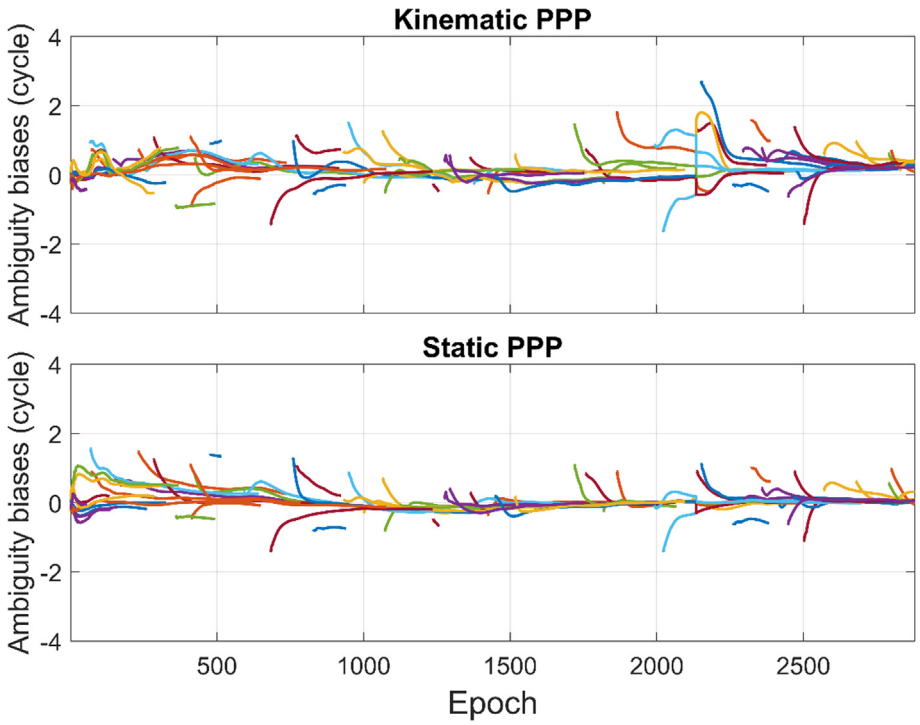

Fig. 13. Ambiguity biases of the first frequency of the kinematic and static PPP caused by the asymmetrical troposphere in the weather event. Each line represents one satellite.

Table 3
Percentages of horizontal SPP and PPP (ambiguity float) positioning biases caused by the asymmetrical troposphere in different cases.

Weather case	Positioning case		$bias < 0.01\ m$	$0.01\ m < bias < 0.1\ m$	$bias > 0.1\ m$
Normal weather	SPP	Epoch by epoch	99.58%	0.42%	0
	PPP	Kinematic	99.62%	0.38%	0
		Static	1	0	0
Weather event	SPP	Epoch by epoch	3.89%	95.21%	0.90%
	PPP	Kinematic	2.71%	97.15%	0.14%
		Static	13.26%	86.74%	0

Table 4
Percentage of 3**D** SPP and PPP (ambiguity float) positioning biases caused by the asymmetrical troposphere in different cases.

Weather case	Positioning case		$bias < 0.01\ m$	$0.01\ m < bias < 0.1\ m$	$bias > 0.1\ m$
Normal weather	SPP	Epoch by epoch	97.81%	2.19%	0
	PPP	Kinematic	97.92%	2.08%	0
		Static	1	0	0
Weather event	SPP	Epoch by epoch	0.21%	91.07%	8.72%
	PPP	Kinematic	0	94.93%	5.07%
		Static	0	96.81%	3.19%

the success rate with the biased ambiguity solutions. Results show that the success rates in the normal weather condition are similar to the ideal troposphere with symmetrical delays. However, users may carefully consider fixing ambiguities in weather event because the actual success rates are extremely low at some epochs in this case study. Since the theoretical success rates cannot take into account the model errors, wrong fixing may occur during a weather event, and in this case the positioning solutions may be affected.

Although we have investigated the influence of the inhomogeneous troposphere on the GNSS estimations and provided the corresponding positioning biases scale and actual integer ambiguity resolution success rate in the presence of the tropospheric model errors in the realistic atmosphere, one should keep in mind that weather events are always too complex to be modelled and analyzed even with the help of NWP models. For instance, the direction of weather front, the total precipitation and the speed of wind may all the factors changing the water vapor content which

leads to an asymmetrical troposphere. Therefore, more data sources may be used in further studies to calibrate the tropospheric contributions and additional noises due to weather events. Besides, the horizontal tropospheric gradients are not considered in this contribution because this study is mainly based on simulations, and only the satellite positions are used in the GNSS observation file. Thus, the gradients are not able to be determined. However, since the gradients can only consider a linear asymmetry of the troposphere in horizontal, the model errors due to the asymmetrical troposphere could be reduced in normal weather condition, but would not change much in weather event due to the complex atmosphere. Following studies may consider using real data to evaluate the influences of the inhomogeneous troposphere on GNSS positioning and integer ambiguity resolution. However, the reference stations must be carefully selected to avoid such influences so that the corrections provided to users can keep unbiased.

Declaration of Competing Interest

The authors declare that they have no known competing financial interests or personal relationships that could have appeared to influence the work reported in this paper.

Acknowledgement

The first and fourth author have received funding from the European Union's Horizon 2020 research and innovation programme under the Marie-Sklodowska Grant Agreement No 722023. This research was also partially supported by National Natural Science Foundation of China (Grant No 41774035). The first author would like to thank Dr Siebren De Haan at Koninklijk Nederlands Meteorologisch Instituut (KNMI) and Dr Han Dun at Delft University of Technology for valuable discussions and precious comments. The author would like to acknowledge the support of International GNSS Service (IGS) for providing the precise satellite orbit products and the support of The Netherlands' Cadastre, Land Registry and Mapping Agency (Kadaster) for maintaining the GNSS network of The Netherlands.

Dataset

GNSS station ADR2: ftp://gnss-data.kadaster.nl/root/data/daily/.

Satellite orbit: ftp://cddis.gsfc.nasa.gov/pub/gps/products/.

References

Angrisano, A., Gaglione, S., Gioia, C., 2013. Performance assessment of GPS/GLONASS single point positioning in an urban environment. Acta Geod. Geophys. 48 (2), 149–161. https://doi.org/10.1007/s40328-012-0010-4.

Bar-Sever, Y.E., Kroger, P.M., Borjesson, J.A., 1998. Estimating horizontal gradients of tropospheric path delay with a single GPS receiver. J. Geophys. Res. Solid Earth. 103 (B3), 5019–5035. https://doi.org/10.1029/97JB03534.

Bertiger, W., Desai, S.D., Haines, B., et al., 2010. Single receiver phase ambiguity resolution with GPS data. J. Geod. 84 (5), 327–337. https://doi.org/10.1007/s00190-010-0371-9.

Bevis, M., Businger, S., Chiswell, S., Herring, T.A., Anthes, R.A., Rocken, C., Ware, R.H., 1994. GPS meteorology: mapping zenith wet delays onto precipitable water. J. Appl. Meteorol. 33 (3), 379–386. https://doi.org/10.1175/1520-0450(1994)033<0379:GMMZWD>2.0.CO;2.

Boehm, J., Heinkelmann, R., Schuh, H., 2007. Short note: a global model of pressure and temperature for geodetic applications. J. Geod. 81 (10), 679–683. https://doi.org/10.1007/s00190-007-0135-3.

Boehm, J., Schuh, H., 2007. Troposphere gradients from the ECMWF in VLBI analysis. J. Geod. 81 (6), 403–408. https://doi.org/10.1007/s00190-007-0144-2.

Boehm, J., Werl, B., Schuh, H., 2006. Troposphere mapping functions for GPS and very long baseline interferometry from European Centre for Medium-Range Weather Forecasts operational analysis data. J. Geophys. Res. Solid Earth. 111 (B2), 406. https://doi.org/10.1029/2005JB003629.

Chen, G., Herring, T., 1997. Effects of atmospheric azimuthal asymmetry on the analysis of space geodetic data. J. Geophys. Res.: Solid Earth 102 (B9), 20489–20502. https://doi.org/10.1029/97JB01739.

de Haan, S., Marseille, G.J., de Valk, P., 2013. Impact of ASCAT scatterometer wind observations on the high-resolution limited-area model (HIRLAM) within an operational context. Weather Forecast. 28 (2), 489–503. https://doi.org/10.1175/WAF-D-12-00056.1.

Dousa, J., Dick, G., Kačmařík, M., Brožková, R., Zus, F., Brenot, H., Kaplon, J., 2016. Benchmark campaign and case study episode in central Europe for development and assessment of advanced GNSS tropospheric models and products. Atmos. Meas. Tech. 9, 2989–3008. https://doi.org/10.5194/amt-9-2989-2016.

Ge, M., Gendt, G., Rothacher, M.A., 2008. Resolution of GPS carrier-phase ambiguities in precise point positioning (PPP) with daily observations. J. Geod. 82 (7), 389–399. https://doi.org/10.1007/s00190-007-0187-4.

Geng, J., Teferle, F.N., Meng, X., 2011. Towards PPP-RTK: ambiguity resolution in real-time precise point positioning. Adv. Space Res. 47 (10), 1664–1673. https://doi.org/10.1016/j.asr.2010.03.030.

Ifadis, I.M., 1992. The excess propagation path of radio waves: Study of the influence of the atmospheric parameters on its elevation dependence. Surv. Rev. 31 (243), 289–298. https://doi.org/10.1179/sre.1992.31.243.289.

Klobuchar, J.A., 1987. Ionospheric time-delay algorithm for single-frequency GPS users. IEEE Trans. Aero Elec. Sys. 23 (3), 325–331. https://doi.org/10.1109/TAES.1987.310829.

Knoop, V.L., de Bakker, P.F., Tiberius, C.C., 2017. Lane determination with GPS precise point positioning. IEEE Trans. Intell. Transp. Syst. 18 (9), 2503–2513. https://doi.org/10.1109/TITS.2016.2632751.

Lagler, K., Schindelegger, M., Böhm, J., 2013. GPT2: Empirical slant delay model for radio space geodetic techniques. Geophys. Res. Lett. 40 (6), 1069–1073. https://doi.org/10.1002/grl.50288.

Landskron, D., Boehm, J., 2018. VMF3/GPT3: refined discrete and empirical troposphere mapping functions. J. Geod. 92 (4), 349–360. https://doi.org/10.1007/s00190-017-1066-2.

Leandro, R., Santos, M.C., Langley, R.B., 2006. UNB neutral atmosphere models: development and performance. In: ION NTM 2006, January 18–20, Monterey, California, USA. pp. 564–573.

Li, B., Verhagen, S., Teunissen, P.J., 2014. Robustness of GNSS integer ambiguity resolution in the presence of atmospheric biases. GPS Solut. 18 (2), 283–296. https://doi.org/10.1007/s10291-013-0329-5.

Ma, H., Verhagen, S., 2020. Precise point positioning on the reliable detection of tropospheric model errors. Sensors 20, 1634. https://doi.org/10.3390/s20061634.

Ma, H., Zhao, Q., Verhagen, S., Psychas, D., Liu, X., 2020. Assessing the performance of multi-GNSS PPP-RTK in the local area. Remote Sens. 12, 3343. https://doi.org/10.3390/rs12203343.

Masoumi, S., McClusky, S., Koulali, A., Tregoning, P., 2017. A directional model of tropospheric horizontal gradients in Global Positioning System and its application for particular weather scenarios. J. Geophys. Res.: Atmos. 122 (8), 4401–4425. https://doi.org/10.1002/2016JD026184.

Meindl, M., Schaer, S., Hugentobler, U., Beutler, G., 2004. Tropospheric gradient estimation at CODE: results from global solutions. J. Meteorol. Soc. Jpn. Ser. II 82 (1B), 331–338. https://doi.org/10.2151/jmsj.2004.331.

Niell, A.E., 1996. Global mapping functions for the atmosphere delay at radio wavelengths. J. Geophys. Res. Solid Earth. 101 (B2), 3227–3246. https://doi.org/10.1029/95JB03048.

Odijk, D., Zhang, B., Khodabandeh, A., 2016. On the estimability of parameters in undifferenced, uncombined GNSS network and PPP-RTK user models by means S-system theory. J. Geod. 90 (1), 15–44. https://doi.org/10.1007/s00190-015-0854-9.

Pelc-Mieczkowska, R., Tomaszewski, D., 2020. Space state representation product evaluation in satellite position and receiver position domain. Sensors 20 (13), 3791. https://doi.org/10.3390/s20133791.

Psychas, D., Bruno, J., Massarweh, L., 2019. Towards sub-meter positioning using Android raw GNSS measurements. In: ION GNSS + 2019, September 16–20, Miami, Florida, USA. pp. 3917–3931.

Psychas, D., Verhagen, S., 2020. Real-time PPP-RTK performance analysis using ionospheric corrections from multi-scale network configurations. Sensors. 20 (11), 3012. https://doi.org/10.3390/s20113012.

Psychas, D., Verhagen, S., Liu, X., 2018. Assessment of ionospheric corrections for PPP-RTK using regional ionosphere modelling. Meas Sci Technol. 30 (1), http://dx.doi.org/10.1088%2F1361-6501%2Faae-fe5 014001.

Saastamoinen, J., 1972. Atmospheric correction for the troposphere and stratosphere in radio ranging satellites. In: Geophysical Monogram Series, American Geophysical Union, Band 15, Washington, D.C., 247–251. https://doi.org/10.1029/GM015p0247.

Schaer, S., Beutler, G., Rothacher, M., 1998. Mapping and predicting the ionosphere. In: IGS Workshop, 1998, February 9–11, Darmstadt, Germany. pp. 1–12.

Smith, E.K., Weintraub, S., 1953. The constants in the equation for atmospheric refractive index at radio frequencies. In: IRE 1953, August, 41(8), 1035–1037. https://doi.org/10.1109/JRPROC.1953.274297.

Steigenberger, P., Tesmer, V., Krügel, M., 2007. Comparisons of homogeneously reprocessed GPS and VLBI long time-series of troposphere zenith delays and gradients. J. Geod. 81 (6), 503–514. https://doi.org/10.1007/s00190-006-0124-y.

Teunissen, P.J., Odijk, D., Zhang, B., 2010. PPP-RTK: results of CORS network-based PPP with integer ambiguity resolution. J. Aeronaut. Astronaut. Aviat. Ser. 42 (4), 223–230 https://gnss.curtin.edu.au/wp-content/uploads/sites/21/2016/04/Teu10.pdf.

Verhagen, S., Li, B., Teunissen, P.J., 2013. Ps-LAMBDA: ambiguity success rate evaluation software for interferometric applications. Comput Geosci. 54, 361–376. https://doi.org/10.1016/j.cageo.2013.01.014.

Verhagen, S., Teunissen, P.J., 2017. Least-squares estimation and Kalman filtering. In: Springer Handbook of Global Navigation Satellite Systems. Springer, Berlin, Heidelberg, Germany, pp. 639–660. https://doi.org/10.1007/978-3-319-42928-1_22.

Wübbena, G., Schmitz, M., Bagge, A., 2005. PPP-RTK: precise point positioning using state-space representation in RTK networks. In: ION GNSS+ 2005, September 13–16, Long Beach, California, USA. pp. 13–16.

Yao, Y., Xu, C., Shi, J., 2015. ITG: A new global GNSS tropospheric correction model. Sci. Rep. 5 (1), 1–9. https://doi.org/10.1038/srep10273.

Zhang, B., Chen, Y., Yuan, Y., 2019. PPP-RTK based on undifferenced and uncombined observations: theoretical and practical aspects. J. Geod. 93 (7), 1011–1024. https://doi.org/10.1007/s00190-018-1220-5.

Zumberge, J.F., Heflin, M.B., Jefferson, D.C., 1997. Precise point positioning for the efficient and robust analysis of GPS data from large networks. J. Geophys. Res. Solid Earth. 102 (B3), 5005–5017. https://doi.org/10.1029/96JB03860.